

# UniLoc: Towards Universal Place Recognition Using Any Single Modality

Yan Xia<sup>\*1,2†</sup> Zhendong Li<sup>\*1</sup> Yun-Jin Li<sup>1</sup> Letian Shi<sup>1</sup> Hu Cao<sup>1</sup> João F. Henriques<sup>3</sup> Daniel Cremers<sup>1,2</sup>

<sup>1</sup>Technical University of Munich <sup>2</sup>Munich Center for Machine Learning (MCML)

<sup>3</sup>Visual Geometry Group, University of Oxford

{yan.xia, zhendong.li, yunjin.li, letian.shi, cao.hu, cremers}@tum.de, joao@robots.ox.ac.uk

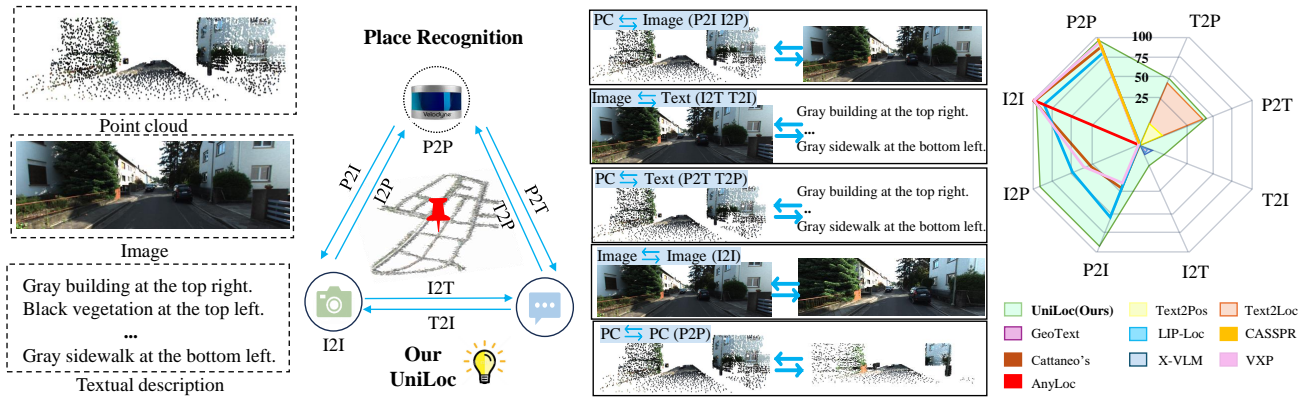


Figure 1. (Left) We present UniLoc, a solution designed for city-scale place recognition using any one of three modalities: text, image, or point cloud. (Right) Localization performance at top-1 recall on the KITTI-360 [21] test set. The proposed UniLoc achieves state-of-the-art performance across all six cross-modality place recognition: image-to-point cloud (I2P), point cloud-to-image (P2I), text-to-point cloud (T2P), point cloud-to-text (P2T), image-to-text (I2T), and text-to-image (T2P). Notably, UniLoc surpasses existing SOTA cross-modal methods by a large margin while achieving competitive performance in uni-modal place recognition.

## Abstract

To date, most place recognition methods focus on single-modality retrieval. While they perform well in specific environments, cross-modal methods offer greater flexibility by allowing seamless switching between map and query sources. It also promises to reduce computation requirements by having a unified model, and achieving greater sample efficiency by sharing parameters. In this work, we develop a universal solution to place recognition, UniLoc, that works with any single query modality (natural language, image, or point cloud). UniLoc leverages recent advances in large-scale contrastive learning, and learns by matching hierarchically at two levels: instance-level matching and scene-level matching. Specifically, we propose a novel Self-Attention based Pooling (SAP) module to evaluate the importance of instance descriptors when aggregated into a place-level descriptor. Experiments on the KITTI-360 dataset demonstrate the benefits of cross-modality for place recognition, achieving superior performance in cross-modal

settings and competitive results also for uni-modal scenarios. Our project page is publicly available at <https://yan-xia.github.io/projects/UniLoc/>.

## 1. Introduction

Place Recognition (PR) is essential for autonomous vehicles and robots, enabling them to self-localize accurately in complex, large-scale environments, such as urban areas or parking structures where buildings or tunnels can block Navigation Satellite System (GNSS) signals. The goal of place recognition is to identify the closest matching location in a pre-built database from a given query that describes the current scene. Given the range of sensors onboard robots, queries can take different forms, including natural language descriptions, RGB images, or LiDAR point clouds.

Usually, the implementation of place recognition is expressed as a retrieval task. Over the past decade, image retrieval-based solutions [1, 3, 15, 25] have shown promising results. However, these methods often struggle with significant variations in lighting, weather, and seasonal ap-

<sup>†</sup>Corresponding author. <sup>\*</sup>Equal contribution.

pearances. As a possible remedy, point cloud based place recognition [2, 17, 36, 38] becomes an attractive research topic since 3D point clouds acquired from LiDAR provide highly accurate, detailed, and illumination-invariant spatial information [37]. Yet, despite its robustness, relying on only a single data source like LiDAR poses limitations, particularly if sensors malfunction or if the sensor setup varies across environments [20].

To address these limitations, cross-modal methods [8, 10, 16, 20, 39, 41] have emerged, offering flexibility by enabling place recognition across different query and map data sources. For example, camera-to-LiDAR approaches [8, 20] support querying a LiDAR database with 2D images, which is beneficial in situations where processing large point clouds is impractical or where LiDAR data is unavailable or compromised. Such approaches reduce computational load and ensure reliable localization even with limited sensor availability. This cross-modal capability is also highly relevant to real-world navigation tasks, such as delivery services, where couriers may rely on verbal directions from recipients to find precise drop-off points. More broadly, the “last mile problem”—navigating to an unfamiliar final destination—highlights the need for flexible place recognition methods that can incorporate natural language input [10, 16, 39, 41]. Despite this demand, there remains no universal place recognition solution that seamlessly integrates text, images, and point clouds.

In this work, we address the question: **how can we design a universal place recognition solution that works regardless of the query modality?** This entails generating shared place representations from a general model by leveraging any single-modal data, including text, image, and point clouds. Unlike ImageBind [13], which is more focused on instance-level retrieval and lacks geographic information, the main challenge in ours lies in mapping the *place-level* descriptors from various modalities into a unified space, enabling consistent and accurate retrieval.

As highlighted by VXP [20], local correspondences are crucial for accurate global localization. Inspired by this, we decompose the place recognition problem into two stages: instance-level matching and scene-level matching. In instance-level matching, we aim to map pairs of modalities—(image, text) and (image, point cloud)—into a shared learning space. The reason is that ImageBind has shown aligning each modality’s embedding to image embeddings results in emergent cross-modal alignment. We focus on fusing multiple modalities and follow recent works that perform learning over large pre-trained models, such as BLIP-2 [19]. In scene-level matching, we find that different instance descriptors should tactically contribute unevenly when aggregated into a place-level descriptor. To achieve this, we develop a Self-Attention based Pooling (SAP) module instead of the max-pooling layers widely used in previous global de-

scriptors [2, 36]. These operations enable one-stage training to map the place-level descriptors from different modalities into a shared embedding space.

To summarize, the main contributions of this work are:

- To the best of our knowledge, we are the first to propose a universal place recognition network for large-scale outdoor environments that can handle any single modality, including natural language, images, or point clouds.
- We propose a novel method UniLoc, leveraging recent advances in large-scale contrastive learning and following hierarchically matching stages.
- We propose a novel self-attention based pooling method that directs the model to focus on the more discriminative instance descriptors during the scene-level matching.
- We conduct extensive experiments on the KITTI-360 data set [21] and show that the proposed UniLoc greatly improves over the state-of-the-art cross-modal methods while achieving competitive performance compared with unimodal methods.

## 2. Related Work

We will focus on the related tasks of visual place recognition, point cloud based place recognition, and cross-modal place recognition between two different modalities.

**Visual place recognition.** Given a query image or image sequence, visual place recognition (VPR) aims to retrieve the closest match to this query on the geo-tagged reference map. The effectiveness of modern VPR methods is primarily due to training in large-scale datasets. NetVLAD [3] achieved excellent performance by employing weakly-supervised contrastive learning with the Pitts250k dataset [31]. Subsequently, DeLF [25] and DeLG [6] explore the large-scale image retrieval tasks supported by the Google-Landmark V1 (1 million images) and V2 (5 million images) datasets [35]. Unlike them, CosPlace [5] explores retrieving as a classification task. MixVPR [1] proposes extracting features using an MLP-based feature mixer. More recently, AnyLoc [15] is the first VPR solution that exhibits anywhere, anytime, and anyview capabilities. However, the performance of VPR often declines under significant variations in illumination and appearance due to changes in weather and seasons.

**Point cloud based place recognition.** Compared with images, point cloud based place recognition provides distinct advantages, remaining robust against variations in lighting, weather, and seasons. PointNetVlad [2] was a pioneering network using end-to-end learning for 3D place recognition. Building on this, SOE-Net [36] introduces the PointOE module, adding orientation encoding to PointNet for point-wise local descriptors. Additionally, several methods [4, 11, 12, 23, 24, 43, 45] incorporate transformer networks with stacked self-attention blocks to capture long-range contextual features. In contrast, Minkloc3D [17] uses

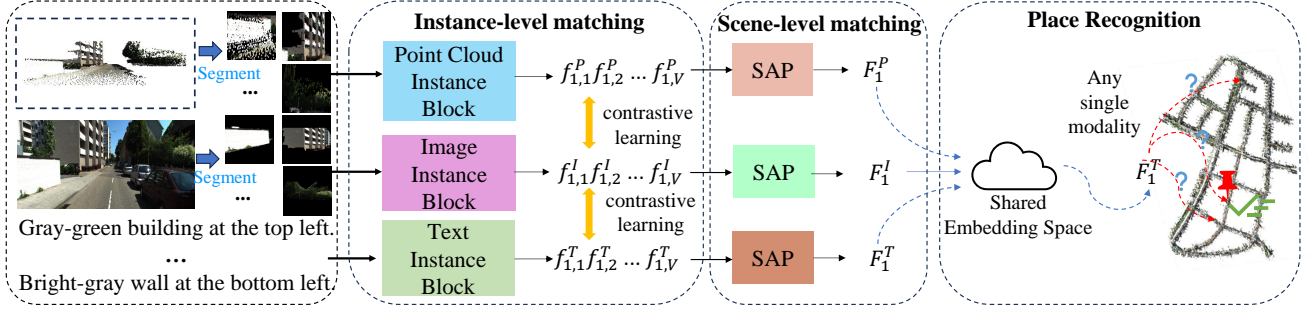


Figure 2. Overview of the proposed pipeline, consisting of instance-level (sec. 4.1) and scene-level (sec. 4.2) matching stages.

a voxel-based approach with a Feature Pyramid Network (FPN)[22] and GeM pooling[27] to create a compact global descriptor, though voxelization can lose points during quantization. To address this, CASSPR [38] introduces a dual-branch hierarchical cross-attention transformer, blending the benefits of voxel- and point-based methods.

**Cross-modal place recognition.** With breakthroughs in large language models (LLM), vision and language localization have become an intense research focus. Language-guided localization requires an agent to follow natural language instructions when localizing in a specific environment. X-VLM [41] achieves Image-Text retrieval by aligning text descriptions with the corresponding visual concepts in images. GeoText [10] is the first work to explore the language-guided drone navigation task by text-to-image and image-to-text retrieval. For Image-LiDAR place recognition, Cattaneo *et al.* [8] first establish a shared global feature space between 2D images and 3D point clouds using a teacher-student model. Recent VXP [20] improves the retrieval performance by enforcing local similarities in a self-supervised manner. In Text-LiDAR point cloud localization, Text2Pos [16] pioneered large-scale outdoor scene localization by first identifying coarse locations and then refining pose estimates. Building on this, Wang *et al.* [34] introduced a Transformer-based approach to improve representation discriminability for both point clouds and text queries. Text2Loc [39] further enhances localization accuracy and efficiency by adopting contrastive learning and a lighter, faster strategy that eliminates the need for a text-instance matcher. In this work, we aim to address the place recognition problem in a unified solution that leverages any single modality independently.

### 3. Problem Statement

We begin by defining the large-scale point cloud reference map  $PC_{\text{ref}} = \{S_i : i = 1, \dots, M\}$ , which is a collection of submaps  $S_i$ . Each 3D submap  $S_i = \{p_{i,j} | j = 1, \dots, n\}$  contains a set of 3D object instances  $p_{i,j}$ . Let  $I_{\text{ref}} = \{I_i | i = 1, \dots, M\}$  represent an image sequence,

where each image  $I_i$  corresponds to the same location as the submap  $S_i$  in  $PC_{\text{ref}}$ . Each 2D image  $I_i = \{o_{i,j} | j = 1, \dots, n\}$  contains a set of 2D object instances  $o_{i,j}$ . In our work, an image  $I_i$  has the same number of object instances as  $S_i$ . Besides, let  $T_{\text{ref}} = \{T_i | i = 1, \dots, M\}$  be text descriptions. Each  $T_i$  includes a set of hints  $\{\vec{h}_k\}_{k=1}^h$ , with each hint describing the spatial position of an object instance in  $I_i$  space.

We approach this task by decomposing it into two stages: instance-level matching and scene-level matching. The instance-level matching stage aims to train a function  $F$  that aligns individual object instances across different modalities. Specifically, we align each 3D object instance  $p_{i,j}$  with its corresponding 2D representation  $o_{i,j}$  and also align the 2D object instance  $o_{i,j}$  with its corresponding text hint  $\vec{h}_k$ . The function  $F$  encodes these 3D, 2D, and textual representations into a unified embedding space. In this embedding space, matching instances across modalities are brought closer together, while non-matching instances are pushed apart. In the context of scene-level matching, we leverage the feature extraction capabilities of the pre-trained instance-level model. The goal is to train a function  $M$  that effectively aggregates the instance-level descriptors into a unified place-level descriptor.

## 4. UniLoc

To the best of our knowledge, our approach, UniLoc, is the first place recognition solution that exhibits any single modality (text, image, or point cloud). Fig. 2 shows the pipeline of our UniLoc. Given a triplet consisting of text descriptions, a single image, and the corresponding 3D submap, we first align the image with the point cloud and the image with the text at the instance level, as detailed in Section 4.1. Next, we aggregate the instance-level descriptors into a place-level representation, as discussed in Section 4.2. The training strategy and loss function are detailed in Section 4.3.

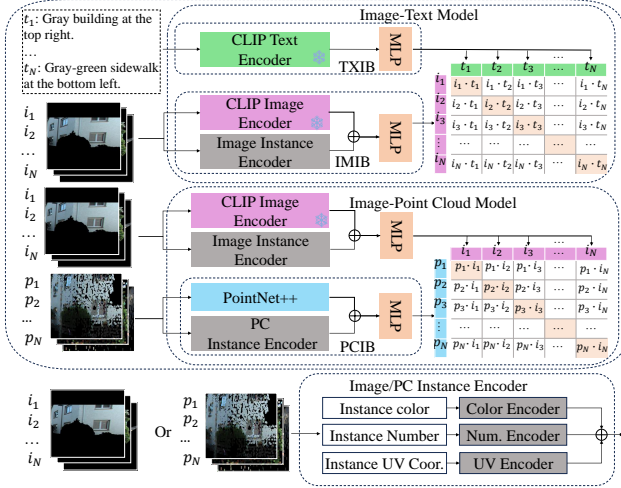


Figure 3. (Top) The architecture of instance-level matching. It consists of three instance-level feature extraction blocks: Text Instance Block (TXIB), Image Instance Block (IMIB), and Point Cloud Instance Block (PCIB). We train an Image-Text and an Image-Point cloud model to align image-text instances and image-point cloud instances, respectively. (Bottom) The architecture of the image and point cloud instance encoders. Note that the pre-trained CLIP image and text encoders are frozen during training.

#### 4.1. Instance-level matching

Considering the stability of training, UniLoc adopts an image-centric approach, where other modalities are embedded into a shared embedding space that aligns closely with the image representation. To achieve this, we employ two instance-level models during the pretraining stage, both centered around image instances: the Image-Text Model and the Image-Point Cloud Model as illustrated in Fig. 3. Below, we provide a detailed explanation of the instance branches that constitute these two models.

**Text branch.** We utilize a pre-trained language encoder in CLIP [28] to extract nuanced features from textual descriptions of object instances. We then design a three-layer MLP to transform the features into a text space  $\mathbf{f}_i^T \in \mathbb{R}^{1 \times D}$ , where  $D$  indicates the feature dimension.

**Image branch.** We use a frozen pre-trained image encoder from CLIP to extract semantic information for each instance, followed by a three-layer MLP to project these features into the image space. Inspired by Text2Loc [39], to capture additional attributes, we utilize an image instance encoder consisting of three components: the Color Encoder, which takes the average RGB values of non-zero regions; the Number Encoder, which uses the normalized count of non-zero pixels; and the UV Encoder, which encodes the average UV coordinates within the original image. Each encoder is a three-layer MLP. Finally, all features are concatenated and passed through another three-layer MLP to produce the im-

age instance descriptor  $\mathbf{f}_i^I \in \mathbb{R}^{1 \times D}$ , where  $D$  indicates the embedding dimension.

**Point cloud branch.** Following [39], we first use PointNet++[26] (although other point networks could also be used) to extract the semantic features from 3D instances. We additionally obtain a color embedding by encoding the average RGB values of the points using a color encoder. We also introduce a number encoder to provide potential class-specific prior information by explicitly encoding the number of points. Unlike Text2Loc [39], we design a novel positional embedding by encoding the UV coordinates of the points (details on the UV coordinate calculation are provided in Section 5), similar to what we used in the image branch. The color, positional, and number encoders are all 3-layer multi-layer perceptrons (MLPs) with output dimensions matching the semantic point embedding dimension. We concatenate the semantic, color, positional, and number embeddings, and then process them with a projection layer, another 3-layer MLP, to obtain the point cloud instance descriptor  $\mathbf{f}_i^P \in \mathbb{R}^{1 \times D}$ .

#### 4.2. Scene-level matching

Following the instance-level matching, we aim to create a shared embedding space between textual descriptions, images, and LiDAR point clouds via aggregating the single-modality instance descriptors to a place-level descriptor. The detailed structures are shown in Fig. 4 (Top). We first load the pre-trained weights from the instance-level matching phase to extract each instance descriptor. Specifically, we use the Image-Text Model weights for the current image and text branches, while the point cloud branch uses the pre-trained weights from the Image-Point Cloud Model. We then introduce a Self-Attention based Pooling (SAP) module to aggregate these instance descriptors into a robust and discriminative scene descriptor.

**Self-Attention based Pooling (SAP).** Inspired by SOE-Net [36], we find that different instance descriptors should have varying importance when aggregating a global scene descriptor. For example, a building can be much less distinctive of a specific scene than a traffic light. We thus propose a self-attention based pooling mechanism intended to replace the previous widely used max-pooling layers in [36]. Multi-Head Self-Attention (MHSA) and FFN sublayers [39] [33] take the instance descriptor  $\mathbf{f}^M$  of any modality  $M$  as input and computes the attention feature  $\mathbf{T}^M \in \mathbb{R}^{V \times D}$ :

$$\tilde{\mathbf{f}}^M = \mathbf{Q} + \text{MSHA}(\mathbf{Q}, \mathbf{K}, \mathbf{V}), \quad (1)$$

$$\mathbf{T}^M = \text{Transformer}(\mathbf{Q}, \mathbf{K}, \mathbf{V}) = \left[ \tilde{\mathbf{f}}^M + \text{FFN}(\tilde{\mathbf{f}}^M) \right] \quad (2)$$

where  $\mathbf{Q}$ ,  $\mathbf{K}$ , and  $\mathbf{V}$  are the query, key, and value matrices respectively, and for simplicity we use the instance descriptor  $\mathbf{f}^M$  to fill their roles:  $\mathbf{Q} = \mathbf{K} = \mathbf{V} = \mathbf{f}^M \in \mathbb{R}^{V \times D}$ , where  $V$  is the number of instances, and  $D$  is the embedding

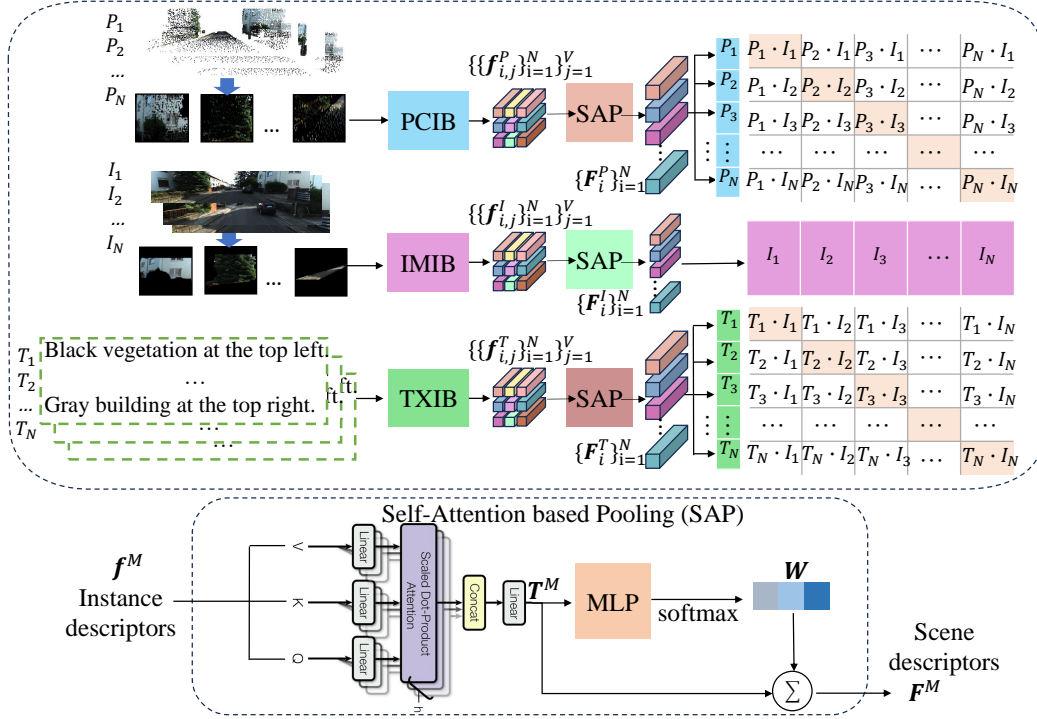


Figure 4. (Top) The proposed fine matching architecture of UniLoc. It consists of triple parallel feature extraction branches: Point cloud, image, and text. (Bottom) The architecture of the proposed Self-Attention based Pooling (SAP) module.

dimension.

We then use a 3-layer MLP and softmax operators to derive attention weights  $\mathbf{W} \in \mathbb{R}^{V \times 1}$  by taking  $\mathbf{T}^M$  as the input:

$$\mathbf{W} = \text{Softmax}(\text{MLP}(\mathbf{T}^M)), \quad (3)$$

The scene descriptor  $\mathbf{F}^M$  is finally obtained by aggregating  $\mathbf{T}^M$  using the attention weights:

$$\mathbf{F}^M = \sum_{i=1}^V \mathbf{W}_i \mathbf{T}_i^M, \quad (4)$$

where  $\mathbf{W}_i$  is the attention weights for the  $i$ -th instance,  $\mathbf{T}_i^M \in \mathbb{R}^{1 \times D}$  is the corresponding attention feature. SAP guides the more important instance descriptors to contribute more to the representation of the target scene descriptor.

### 4.3. Loss function

**Instance-level matching.** We use instance pairs  $(I_{ins}, T_{ins}, P_{ins})$ , where  $I_{ins}$  and  $P_{ins}$  represent the 2D and 3D instances, respectively, and  $T_{ins}$  represents the textual description of the instances. The contrastive loss [28] between  $(I_{ins}, T_{ins})$  can be calculated using the following formula:

$$l(i, I_{ins}, T_{ins}) = -\log \frac{\exp(\mathbf{f}_i^I \cdot \mathbf{f}_i^T / \tau)}{\sum_{j \in N} \exp(\mathbf{f}_i^I \cdot \mathbf{f}_j^T / \tau)} - \log \frac{\exp(\mathbf{f}_i^T \cdot \mathbf{f}_i^I / \tau)}{\sum_{j \in N} \exp(\mathbf{f}_i^T \cdot \mathbf{f}_j^I / \tau)} \quad (5)$$

where  $\mathbf{f}_i^I$  represents the image instance descriptors, and  $\mathbf{f}_i^T$  denotes the descriptors of the corresponding text.  $N$  is the batch size, and  $\tau$  is a temperature parameter. The batch loss during training is obtained by averaging each contrastive loss term:

$$L(I_{ins}, T_{ins}) = \frac{1}{N} \left[ \sum_{i \in N} l(i, I, T) \right] \quad (6)$$

Similarly,  $L(I_{ins}, P_{ins})$  can be derived in the same way.

**Scene-level matching.** As a modality that is inexpensive to collect, images can easily align with various sensory modalities. Specifically, for our task, a large amount of image data, such as Google Maps imagery, is available for aligning with point cloud and textual data. Given these reasons, similar to [13], we adopt an image-centric approach where other modalities align through image embeddings, effectively creating a shared embedding space.

We use pairs  $(I, T)$ , where  $I$  represents images and  $T$  represents the corresponding textual descriptions. The contrastive loss between images and text can be calculated using the following formula:

$$l(i, I, T) = -\log \frac{\exp(F_i^I \cdot F_i^T / \tau)}{\sum_{j \in N} \exp(F_i^I \cdot F_j^T / \tau)} - \log \frac{\exp(F_i^T \cdot F_i^I / \tau)}{\sum_{j \in N} \exp(F_i^T \cdot F_j^I / \tau)} \quad (7)$$

where  $F_i^I$  represents the image descriptor, and  $F_i^T$  denotes the corresponding text descriptor.  $N$  is the batch size. The batch loss during training is obtained by averaging each contrastive loss term:

$$L(I, T) = \frac{1}{N} \left[ \sum_{i \in N} l(i, I, T) \right] \quad (8)$$

$L_S(I, P)$  can be derived in the same way.

Similar to [40], we combine the contrastive loss between images and point clouds and between images and texts through a weighted approach to achieve alignment and proximity among the three modalities in the embedding space:

$$L_{final} = \alpha L(I, T) + (1 - \alpha) L(I, P) \quad (9)$$

where  $L(I, T)$  and  $L(I, P)$  represent the contrastive losses of image-text and image-point cloud pairs,  $\alpha$  is the hyperparameters to balance their relationship.

## 5. Experimental Dataset

Following [39], we use nine sequences from the KITTI-360 dataset [21] as experimental data, with five sequences (00, 02, 04, 06, 07) for training, one (10) for validation, and three (03, 05, 09) for testing. The KITTI-360 dataset spans a driving distance of 80 km with a total coverage area of 15.51 km<sup>2</sup>. Additionally, KITTI-360 labels static objects (e.g., poles, buildings, fences, garages), which makes it particularly suitable for our task. We establish a one-to-one correspondence among the point clouds, text descriptions, and images. To ensure sufficient textual descriptions for image-text and point cloud-text retrieval in both training and evaluation, we filtered out data with fewer than six instances following [39]. In total, we obtain 19,866 triplets of text, image, and point cloud data for training, 1,781 triplets for validation, and 7,791 triplets for testing. More details are in Appendix A.

**Images.** In the training stage, we segment each instance in the raw image using ground-truth semantic labels. To align textual descriptions accurately with instances, we identify connected regions in the instance mask and select the largest as the instance mask. Instances with fewer than 50 valid pixels were deemed unobservable and excluded. The segmented regions are then resized to 224×224, maintaining the aspect ratio and padding with zeros as needed. We use an off-the-shelf segmentation network PSPNet [44] for image segmentation during inference, in the text-image modalities experiment.

**Point clouds.** We initially sample point clouds within a 40 m radius centered on the location of each image. Using the camera’s pose matrix, we transform these points into the camera’s coordinate system and project them onto the image plane using intrinsic parameters to obtain UV coordinates.

We then extract the point cloud segments corresponding to each image instance by utilizing the image bounding boxes and the semantic IDs of the point cloud points. Instances too small to have valid point cloud projections are excluded from both datasets.

**Text.** We describe each image and 3D submap by combining text descriptions of its instances. Each instance’s text hint includes the color, category, and position information. The average RGB values of each instance in the image are used for color description. We assign the category description based on the ground-truth semantic label. For the position, we define six regions based on the average UV coordinates of each instance. We divide the V-axis into “top” and “bottom” and the U-axis into “left” (0 to 0.4 times the image width), “center” (0.4 to 0.6), and “right” (0.6 to 1).

## 6. Experiments

### 6.1. Evaluation criteria

Following [39], we evaluate the place recognition capability of our UniLoc across different modalities or within the same modality using Retrieval Recall at Top  $k$  ( $k \in 1, 3, 5$ ). For a fair comparison in Image-LiDAR, Image-Image, and LiDAR-LiDAR place recognition, we regard the retrieved scan as a correct match if the distance is within 20 m, following [2, 15, 20]. For Text-Image and Text-LiDAR place recognition, retrieving only the image/point cloud at the exact location is considered successful.

### 6.2. Results

#### 6.2.1. Text-Image place recognition

We compare our UniLoc with state-of-the-art image-text retrieval methods X-VLM [41] and GeoText [10] on the test set. Fig. 5 shows the top 1/3/5 recall of each method. UniLoc achieves the best performance across all recall levels. For Text-to-Image retrieval, UniLoc outperforms the recall achieved by the fine-tuned X-VLM by a wide margin of 6.4% at top-1. Furthermore, for the Image-to-Text retrieval, UniLoc surpasses X-VLM with increases of 6.3%, 11.7%, and 14.2% on the test set at top-1/3/5, respectively. These consistent improvements demonstrate our UniLoc marks a clear advancement in the Text-Image place recognition tasks.

#### 6.2.2. Text-LiDAR place recognition

We compare our UniLoc with state-of-the-art Text-LiDAR methods Text2Pos [16] and Text2Loc [39], both with and without our UV Encoder. As shown in Fig. 6, UniLoc achieves the best performance across all recall at top-1/3/5. For Text-to-Lidar retrieval, UniLoc demonstrates notable improvements, surpassing the best-performing Text2Loc by 2.9% at top-1 on the test set. Moreover, for Lidar-to-Text retrieval, UniLoc outperforms other methods, with improvements of 1.5% at top-1 on the test set compared to the

Table 1. Performance comparison for Image-LiDAR place recognition on the KITTI-360 dataset.

Methods	LiDAR-to-Image						Image-to-LiDAR					
	val			test			val			test		
	R@1	R@3	R@5	R@1	R@3	R@5	R@1	R@3	R@5	R@1	R@3	R@5
LIP-Loc [30]	48.2	61.8	66.7	54.0	67.8	75.1	49.4	62.5	70.9	49.3	64.1	70.9
Cattaneo[9]	11.2	17.6	21.3	21.8	28.4	33.5	18.8	31.9	38.9	25.3	36.8	43.7
VXP [20]	33.5	37.3	40.8	19.7	26.1	29.1	43.5	55.5	61.8	31.9	42.7	48.0
UniLoc (Ours)	<b>91.8</b>	<b>95.7</b>	<b>96.3</b>	<b>94.4</b>	<b>97.5</b>	<b>98.0</b>	<b>92.0</b>	<b>96.0</b>	<b>97.4</b>	<b>93.5</b>	<b>96.5</b>	<b>97.7</b>

Table 2. Performance comparison for Image-Image and LiDAR-LiDAR place recognition on the KITTI-360 dataset.

Methods	Image-to-Image						LiDAR-to-LiDAR					
	val			test			val			test		
	R@1	R@3	R@5	R@1	R@3	R@5	R@1	R@3	R@5	R@1	R@3	R@5
LIP-Loc [30]	85.3	93.2	95.3	87.7	94.1	96.0	85.7	92.3	93.9	82.2	89.8	92.4
Cattaneo’s [9]	100	100	100	99.9	99.9	100	95.6	96.3	96.5	90.5	93.8	94.6
VXP [20]	100	100	100	99.9	99.9	99.9	98.3	98.8	99.3	96.5	97.8	98.2
CASSPR [38]	-	-	-	-	-	-	98.8	99.3	99.7	98.1	99.3	99.4
AnyLoc[15]	100	100	100	99.8	99.9	99.9	-	-	-	-	-	-
MixVPR[1]	100	100	100	99.9	99.9	100	-	-	-	-	-	-
UniLoc (Ours)	96.7	99.3	99.7	96.5	98.5	98.9	96.9	98.8	99.0	97.2	99.1	99.2

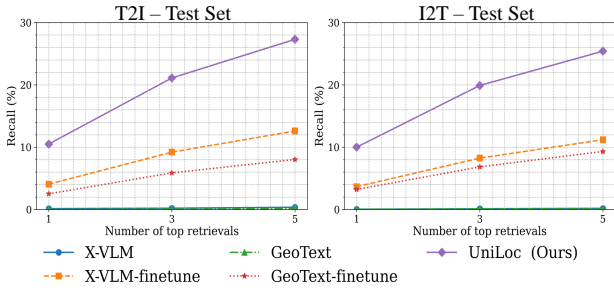


Figure 5. Performance comparison for Text-Image place recognition on the KITTI-360 dataset. "X-VLM/GeoText-finetune" indicates that we finetune the model on the KITTI-360 dataset.

Text2Loc w/UV Encoder configuration. These results underscore UniLoc’s strong retrieval performance, demonstrating its robustness and effectiveness in handling Text-to-LiDAR retrieval tasks.

### 6.2.3. Image-LiDAR place recognition

We compare our UniLoc with state-of-the-art Image-LiDAR models, including LIP-Loc [30], Cattaneo’s [9], and VXP [20]. As shown in Table 1, UniLoc significantly improves over existing models in the Image-LiDAR place recognition task across all recall levels. For LiDAR-to-Image retrieval, UniLoc outperforms other methods by achieving gains of 43.6%, 33.9%, and 29.6% at top-1/3/5 on the validation set, and 40.4%, 29.7%, and 22.9% on the test set, when compared to the best-performing baseline, LIP-Loc. For Image-to-LiDAR retrieval, UniLoc demonstrates notable

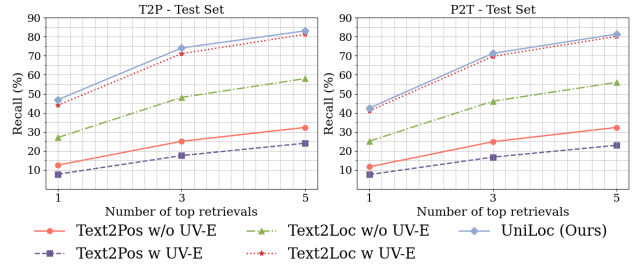


Figure 6. Performance comparison for Text-LiDAR place recognition on the KITTI-360 dataset. "w/o UV-E" indicates removing the UV encoder in the instance encoder and the instance position descriptor in the text, while "w UV-E" indicates the opposite setup.

advancements, surpassing LIP-Loc with increases of 42.6% and 44.2% at top-1 on the validation and test set, respectively. These marked improvements underscore UniLoc’s superior retrieval capabilities, highlighting its robustness and accuracy in Image-LiDAR retrieval tasks.

### 6.2.4. Image-based and LiDAR-based place recognition

We further compare UniLoc with several state-of-the-art unimodal models, including 3D-3D model CASSPR [38] and 2D-2D models AnyLoc [15] and MixVPR [1]. Additionally, we compare with leading 2D-3D models VXP [20], Cattaneo’s [9], and LIP-Loc [30]. As shown in Table 2, UniLoc achieves competitive performance in Image-to-Image and LiDAR-to-LiDAR retrieval tasks. For image-based place recognition, UniLoc achieves the top-1 recall rate of 96.5 on the test set. Additionally, UniLoc reaches 97.2 recall at top-1

Table 3. Ablation study of our UniLoc on the KITTI-360 dataset. "w/o SAP" indicates replacing the proposed self-attention based pooling (SAP) module with the max-pooling layer. "w/o UV-E" indicates removing all encoding modules related to UV coordinates. "w/o pre-trained" indicates not loading the pre-trained weights from instance-level matching stage. "w/o CLIP" indicates replacing the pre-trained CLIP image and text encoder with DINO [42] and T5 [29].

Methods	val				test			
	R@1	R@3	R@5	Ave	R@1	R@3	R@5	Ave
w/o SAP	61.7	86.3	92.9	80.3	73.7	94.3	97.6	88.5
w/o UV-E	46.9	72.9	81.9	67.2	57.6	81.5	87.8	75.6
w/o pre-trained	62.7	86.6	92.8	80.7	71.3	92.4	96.2	86.6
w/o CLIP	56.7	82.2	90.1	76.3	67.0	89.9	94.6	83.8
UniLoc (Ours)	<b>65.6</b>	<b>89.1</b>	<b>94.3</b>	<b>83.0</b>	<b>75.5</b>	<b>95.1</b>	<b>97.9</b>	<b>89.5</b>

for LiDAR-based place recognition. That demonstrates that UniLoc achieves the better performance compared to the previous cross-modal methods.

### 6.3. Ablation study

In this section, we analyze the hyperparameter selection in scene-level matching and evaluate the effectiveness of various components of UniLoc. The results in Table 3 are obtained by averaging the performance on the Text-Image and Image-LiDAR place recognition. All experiments are conducted using 2D ground truth segmentation labels.

**Effectiveness of various components.** To validate the effectiveness of each component in UniLoc, we conduct a series of ablation studies: replacing self-attention based pooling with max pooling in the SAP module (as presented in Section 4.2), removing the UV encoder (presented in Section 4.1) and the instance position descriptor in text, not loading the pre-trained instance-level model during UniLoc training, and substituting the CLIP image and text encoders with DINO [7] and T5 [29]. All networks are trained on the KITTI-360 dataset, with results summarized in Table 3. The experimental results indicate that the self-attention based pooling module enhances the model’s average recall by 2.7% on the validation set and 1% on the test set. Furthermore, incorporating object location descriptions in the text and using the UV encoder increases the model’s average recall by 15.8% on the validation set and 13.9% on the test set. Additionally, the findings reveal that loading the pre-trained instance-level network improves the model’s average recall by 2.3% on the validation set and 2.9% on the test set. Due to the superior alignment capabilities between images and text in CLIP, compared to DINO+T5, using CLIP enhances the model’s average recall by 6.7% on the validation set and 5.7% on the test set.

### 6.4. Computational cost analysis

In this section, we analyze the required computational resources of our UniLoc regarding the number of parameters

and time efficiency. As shown in Table 4, the total parameter count of UniLoc (excluding the parameters from the pre-trained CLIP image and text encoders) is 22.5 M. UniLoc comprises 12.1 M, 3.4 M, and 7.1 M parameters for the point cloud, text, and image branches, respectively. Using a single NVIDIA A40 (48G) GPU, the point cloud instance block in UniLoc requires 2.2 ms to compute a 3D instance-level descriptor and 0.8 ms to aggregate them into a scene-level descriptor. For text, it takes 0.082 ms for instance-level computation and 0.59 ms for aggregation. The image instance block takes 12.6 ms for instance-level computation and 0.66 ms for aggregation.

Table 4. Computational cost requirement analysis of our UniLoc on the KITTI-360 test dataset.

Branch	Parameters (M)			Time Usage (ms)	
	Total	Instance Block	SAP	Instance Descriptor	Scene Descriptor
Point Cloud	12.1	8.7	3.4	2.2	0.8
Image	7.1	3.7	3.4	12.6	0.66
Text	3.4	0.8	2.6	0.082	0.59

### 6.5. Embedding space analysis

We employ T-SNE [32] to visually represent the learned embedding space, as illustrated in Fig. 7. The baseline method LIP-Loc [30] produces a less discriminative embedding space, where positive LiDAR samples are often far from the query images and scattered throughout the space. In contrast, our UniLoc brings positive point cloud samples and query images significantly closer within the embedding space, demonstrating that UniLoc creates a more discriminative cross-modal space for place recognition.

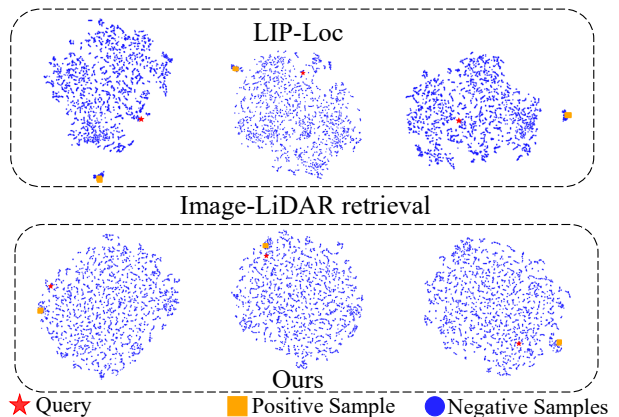


Figure 7. T-SNE visualization for the Image-LiDAR recognition.

## 7. Conclusion

We have presented UniLoc, a method for cross-modal place recognition that can also operate competitively on a single



modality at a time. Our experiments show that factoring the place recognition problem into instance and scene levels for different modalities is an effective solution for place recognition. We hope that cross-modal place recognition results in more robust systems in the future, capable of coping with the loss of different sensors (e.g. under adversarial lighting conditions) and locating a place via natural language descriptions seamlessly. Future work could include explorations of other modalities, such as sound, infrared or even event cameras.

## References

- [1] Amar Ali-Bey, Brahim Chaib-Draa, and Philippe Giguere. Mixvpr: Feature mixing for visual place recognition. In *Proceedings of the IEEE/CVF winter conference on applications of computer vision*, pages 2998–3007, 2023. 1, 2, 7
- [2] Mikaela Angelina Uy and Gim Hee Lee. Pointnetvlad: Deep point cloud based retrieval for large-scale place recognition. In *Proceedings of the IEEE Conference on Computer Vision and Pattern Recognition*, pages 4470–4479, 2018. 2, 6
- [3] Relja Arandjelovic, Petr Gronat, Akihiko Torii, Tomas Pfister, and Josef Sivic. Netvlad: Cnn architecture for weakly supervised place recognition. In *Proceedings of the IEEE conference on computer vision and pattern recognition*, pages 5297–5307, 2016. 1, 2
- [4] Tiago Barros, Luís Garrote, Ricardo Pereira, Cristiano Prevedida, and Urbano J Nunes. Attdlnet: Attention-based deep network for 3d lidar place recognition. In *Iberian Robotics conference*, pages 309–320. Springer, 2022. 2
- [5] Gabriele Berton, Carlo Masone, and Barbara Caputo. Re-thinking visual geo-localization for large-scale applications. In *Proceedings of the IEEE/CVF Conference on Computer Vision and Pattern Recognition*, pages 4878–4888, 2022. 2
- [6] Bingyi Cao, Andre Araujo, and Jack Sim. Unifying deep local and global features for image search. In *Computer Vision—ECCV 2020: 16th European Conference, Glasgow, UK, August 23–28, 2020, Proceedings, Part XX 16*, pages 726–743. Springer, 2020. 2
- [7] Mathilde Caron, Hugo Touvron, Ishan Misra, Hervé Jégou, Julien Mairal, Piotr Bojanowski, and Armand Joulin. Emerging properties in self-supervised vision transformers. In *Proceedings of the IEEE/CVF international conference on computer vision*, pages 9650–9660, 2021. 8
- [8] Daniele Cattaneo, Matteo Vaghi, Simone Fontana, Augusto Luis Ballardini, and Domenico Giorgio Sorrenti. Global visual localization in lidar-maps through shared 2d-3d embedding space. In *International Conference on Robotics and Automation (ICRA)*, pages 4365–4371, 2020. 2, 3
- [9] Daniele Cattaneo, Matteo Vaghi, Simone Fontana, Augusto Luis Ballardini, and Domenico G Sorrenti. Global visual localization in lidar-maps through shared 2d-3d embedding space. In *2020 IEEE International Conference on Robotics and Automation (ICRA)*, pages 4365–4371. IEEE, 2020. 7
- [10] Meng Chu, Zhedong Zheng, Wei Ji, Tingyu Wang, and Tat-Seng Chua. Towards natural language-guided drones: Geotext-1652 benchmark with spatial relation matching. In *European Conference on Computer Vision*, pages 213–231. Springer, 2025. 2, 3, 6
- [11] Haowen Deng, Tolga Birdal, and Slobodan Ilic. Ppfnet: Global context aware local features for robust 3d point matching. In *Proceedings of the IEEE Conference on Computer Vision and Pattern Recognition*, pages 195–205, 2018. 2
- [12] Zhaoxin Fan, Zhenbo Song, Hongyan Liu, Zhiwu Lu, Jun He, and Xiaoyong Du. Svt-net: Super light-weight sparse voxel transformer for large scale place recognition. AAAI, 2022. 2
- [13] Rohit Girdhar, Alaaeldin El-Nouby, Zhuang Liu, Mannat Singh, Kalyan Vasudev Alwala, Armand Joulin, and Ishan Misra. Imagebind: One embedding space to bind them all. In *Proceedings of the IEEE/CVF Conference on Computer Vision and Pattern Recognition*, pages 15180–15190, 2023. 2, 5
- [14] Kaiming He, Xiangyu Zhang, Shaoqing Ren, and Jian Sun. Deep residual learning for image recognition. In *Proceedings of the IEEE conference on computer vision and pattern recognition*, pages 770–778, 2016. 2
- [15] Nikhil Keetha, Avneesh Mishra, Jay Karhade, Krishna Murthy Jatavallabhula, Sebastian Scherer, Madhava Krishna, and Sourav Garg. Anyloc: Towards universal visual place recognition. *IEEE Robotics and Automation Letters*, 2023. 1, 2, 6, 7
- [16] Manuel Kolmet, Qunjie Zhou, Aljoša Ošep, and Laura Leal-Taixé. Text2pos: Text-to-point-cloud cross-modal localization. In *Proceedings of the IEEE/CVF Conference on Computer Vision and Pattern Recognition*, pages 6687–6696, 2022. 2, 3, 6, 1
- [17] Jacek Komorowski. Minkloc3d: Point cloud based large-scale place recognition. In *Proceedings of the IEEE/CVF Winter Conference on Applications of Computer Vision*, pages 1790–1799, 2021. 2
- [18] Junnan Li, Dongxu Li, Caiming Xiong, and Steven Hoi. Blip: Bootstrapping language-image pre-training for unified vision-language understanding and generation. In *International conference on machine learning*, pages 12888–12900. PMLR, 2022. 4
- [19] Junnan Li, Dongxu Li, Silvio Savarese, and Steven Hoi. Blip-2: Bootstrapping language-image pre-training with frozen image encoders and large language models. In *International conference on machine learning*, pages 19730–19742. PMLR, 2023. 2, 4
- [20] Yun-Jin Li, Mariia Gladkova, Yan Xia, Rui Wang, and Daniel Cremers. Vxp: Voxel-cross-pixel large-scale image-lidar place recognition. In *2025 International Conference on 3D Vision (3DV)*, 2025. 2, 3, 6, 7
- [21] Yiyi Liao, Jun Xie, and Andreas Geiger. Kitti-360: A novel dataset and benchmarks for urban scene understanding in 2d and 3d. *IEEE Transactions on Pattern Analysis and Machine Intelligence*, 45(3):3292–3310, 2022. 1, 2, 6
- [22] Tsung-Yi Lin, Piotr Dollár, Ross Girshick, Kaiming He, Bharath Hariharan, and Serge Belongie. Feature pyramid networks for object detection. In *Proceedings of the IEEE Conference on Computer Vision and Pattern Recognition*, pages 2117–2125, 2017. 3

- [23] Junyi Ma, Jun Zhang, Jintao Xu, Rui Ai, Weihao Gu, and Xieyuanli Chen. Overlaptransformer: An efficient and yaw-angle-invariant transformer network for lidar-based place recognition. *IEEE Robotics and Automation Letters*, 7(3): 6958–6965, 2022. 2
- [24] Junyi Ma, Guangming Xiong, Jingyi Xu, and Xieyuanli Chen. Cvtnet: A cross-view transformer network for place recognition using lidar data. *arXiv preprint arXiv:2302.01665*, 2023. 2
- [25] Hyeonwoo Noh, Andre Araujo, Jack Sim, Tobias Weyand, and Bohyung Han. Large-scale image retrieval with attentive deep local features. In *Proceedings of the IEEE international conference on computer vision*, pages 3456–3465, 2017. 1, 2
- [26] Charles R Qi, Hao Su, Kaichun Mo, and Leonidas J Guibas. Pointnet: Deep learning on point sets for 3d classification and segmentation. In *Proceedings of the IEEE conference on computer vision and pattern recognition*, pages 652–660, 2017. 4, 1
- [27] Filip Radenović, Giorgos Tolias, and Ondřej Chum. Fine-tuning cnn image retrieval with no human annotation. *IEEE transactions on pattern analysis and machine intelligence*, 41(7):1655–1668, 2018. 3
- [28] Alec Radford, Jong Wook Kim, Chris Hallacy, Aditya Ramesh, Gabriel Goh, Sandhini Agarwal, Girish Sastry, Amanda Askell, Pamela Mishkin, Jack Clark, et al. Learning transferable visual models from natural language supervision. In *International conference on machine learning*, pages 8748–8763. PMLR, 2021. 4, 5
- [29] Colin Raffel, Noam Shazeer, Adam Roberts, Katherine Lee, Sharan Narang, Michael Matena, Yanqi Zhou, Wei Li, and Peter J Liu. Exploring the limits of transfer learning with a unified text-to-text transformer. *Journal of machine learning research*, 21(140):1–67, 2020. 8
- [30] Sai Shubodh, Mohammad Omama, Husain Zaidi, Udit Singh Parihar, and Madhava Krishna. Lip-loc: Lidar image pre-training for cross-modal localization. In *Proceedings of the IEEE/CVF Winter Conference on Applications of Computer Vision*, pages 948–957, 2024. 7, 8
- [31] Akihiko Torii, Josef Sivic, Tomas Pajdla, and Masatoshi Okutomi. Visual place recognition with repetitive structures. In *Proceedings of the IEEE conference on computer vision and pattern recognition*, pages 883–890, 2013. 2
- [32] Laurens Van der Maaten and Geoffrey Hinton. Visualizing data using t-sne. *JMLR*, 2008. 8
- [33] A Vaswani. Attention is all you need. *Advances in Neural Information Processing Systems*, 2017. 4
- [34] Guangzhi Wang, Hehe Fan, and Mohan Kankanhalli. Text to point cloud localization with relation-enhanced transformer. *arXiv preprint arXiv:2301.05372*, 2023. 3
- [35] Tobias Weyand, Andre Araujo, Bingyi Cao, and Jack Sim. Google landmarks dataset v2-a large-scale benchmark for instance-level recognition and retrieval. In *Proceedings of the IEEE/CVF conference on computer vision and pattern recognition*, pages 2575–2584, 2020. 2
- [36] Yan Xia, Yusheng Xu, Shuang Li, Rui Wang, Juan Du, Daniel Cremers, and Uwe Stilla. Soe-net: A self-attention and orientation encoding network for point cloud based place recognition. In *Proceedings of the IEEE/CVF Conference on computer vision and pattern recognition*, pages 11348–11357, 2021. 2, 4
- [37] Yan Xia, Yusheng Xu, Cheng Wang, and Uwe Stilla. Vpc-net: Completion of 3d vehicles from mls point clouds. *ISPRS Journal of Photogrammetry and Remote Sensing*, 174:166–181, 2021. 2
- [38] Yan Xia, Mariia Gladkova, Rui Wang, Qianyun Li, Uwe Stilla, João F Henriques, and Daniel Cremers. Casspr: Cross attention single scan place recognition. In *Proceedings of the IEEE/CVF International Conference on Computer Vision (ICCV)*, pages 8461–8472, 2023. 2, 3, 7
- [39] Yan Xia, Letian Shi, Zifeng Ding, Joao F Henriques, and Daniel Cremers. Text2loc: 3d point cloud localization from natural language. In *Proceedings of the IEEE/CVF Conference on Computer Vision and Pattern Recognition*, pages 14958–14967, 2024. 2, 3, 4, 6, 1
- [40] Le Xue, Mingfei Gao, Chen Xing, Roberto Martín-Martín, Jiajun Wu, Caiming Xiong, Ran Xu, Juan Carlos Niebles, and Silvio Savarese. Ulip: Learning a unified representation of language, images, and point clouds for 3d understanding. In *Proceedings of the IEEE/CVF conference on computer vision and pattern recognition*, pages 1179–1189, 2023. 6
- [41] Yan Zeng, Xinsong Zhang, and Hang Li. Multi-grained vision language pre-training: Aligning texts with visual concepts. In *International Conference on Machine Learning*, pages 25994–26009. PMLR, 2022. 2, 3, 6
- [42] Hao Zhang, Feng Li, Shilong Liu, Lei Zhang, Hang Su, Jun Zhu, Lionel M Ni, and Heung-Yeung Shum. Dino: Detr with improved denoising anchor boxes for end-to-end object detection. *arXiv preprint arXiv:2203.03605*, 2022. 8
- [43] Wenxiao Zhang, Huajian Zhou, Zhen Dong, Qingan Yan, and Chunxia Xiao. Rank-pointretrieval: Reranking point cloud retrieval via a visually consistent registration evaluation. *IEEE Transactions on Visualization and Computer Graphics*, 2022. 2
- [44] Hengshuang Zhao, Jianping Shi, Xiaojuan Qi, Xiaogang Wang, and Jiaya Jia. Pyramid scene parsing network. In *Proceedings of the IEEE conference on computer vision and pattern recognition*, pages 2881–2890, 2017. 6, 2
- [45] Zhicheng Zhou, Cheng Zhao, Daniel Adolphsson, Songzhi Su, Yang Gao, Tom Duckett, and Li Sun. Ndt-transformer: Large-scale 3d point cloud localisation using the normal distribution transform representation. In *2021 IEEE International Conference on Robotics and Automation (ICRA)*, pages 5654–5660. IEEE, 2021. 2

# UniLoc: Towards Universal Place Recognition Using Any Single Modality

## Supplementary Material

In this Supplementary Material, we present extensive additional experiments conducted on the KITTI-360 dataset, further illustrating the effectiveness of UniLoc. Additionally, we provide detailed insights into the experimental setup and dataset. In Sec. A, we discuss the dataset generation process and its key specifics. Sec. B highlights implementation details, clarifying the methods employed. In Sec. C, we offer a qualitative analysis of the top-3 candidate retrieved results, demonstrating their place recognition performance across diverse tasks. Lastly, Sec. D presents additional ablation studies to rigorously validate the robustness and general effectiveness of our UniLoc. **We also provide our code for reproducibility in this Supp. Submission.**

### A. Dataset Details

**Dataset trajectory distribution.** To ensure a one-to-one correspondence between the textual descriptions and the image and point cloud data in the place recognition tasks, we deduplicated the dataset using text descriptions generated from the images, maintaining a minimum distance of one meter between scenes. Fig. 8 depicts the spatial distribution of trajectories across the dataset, while Fig. 9 highlights the distribution of test and validation data used in the experiments for Tab. 1 and 2. (in main paper). A test region refers to a specific area within the dataset designated for generating queries to evaluate the model’s retrieval performance. For sequences 03, 09, and 10, distinct test regions were defined, and queries were restricted to these areas. In the case of sequence 05, its close proximity to the training data from sequences 04 and 06 made it challenging to define non-overlapping test regions. As a result, every data point in sequence 05 is treated as a query, effectively treating the entire sequence as a test region.

**Pre-processing of point cloud.** Most automotive datasets focus primarily on the instance segmentation of dynamic objects such as vehicles and pedestrians. In contrast, KITTI360 expands its annotation scope to include static object categories like buildings and traffic lights. These static objects provide consistent and reliable references, making them particularly valuable for localization tasks. Similar to [16][39], in this work, we exploit static object instances not only to generate position queries but also as essential cues to improve the accuracy and robustness of position localization. We utilize the semantic IDs in the KITTI-360 dataset’s Accumulated Point Clouds to filter the desired object classes. Using instance IDs, we further distinguish and aggregate all instances within each class into individual objects. At this

stage, each object in the point cloud is assigned a unique and consistent instance ID. However, this processing results in numerous objects for each class. The purpose of this step is to aggregate objects and downsample them according to their class. For instance, buildings are downsampled using a voxel size of 0.25, while poles are not downsampled. This approach ensures that objects from different classes maintain a roughly consistent number of points. Additionally, we filter out objects with fewer points than a class-specific threshold (e.g., buildings require at least 250 points, while poles require a minimum of 25 points). Subsequently, we sample the processed Accumulated Point Clouds using a 40-meter radius around the positions of images in the dataset. During this process, smaller objects that lose more than one-third of their points due to sampling are discarded. This decision is made because PointNet++ [26] struggles to capture the semantic information of small objects (e.g., lamps, trash bins) with significant point cloud loss. Notably, to ensure the average color of the point clouds aligns with the textual descriptions derived from the corresponding images, the RGB color of each point is assigned based on the pixel value at its projected UV coordinates in the image. The remaining steps of the processing pipeline have already been described in detail in the main paper.

Each scene is designed to include a fixed 12 instances. For scenes containing more than 12 instances, instances are randomly filtered to retain only 12. Notably, all text-related experiments (Text-to-LiDAR, LiDAR-to-Text, Text-to-Image, and Image-to-Text) utilize text generated directly from the images. Furthermore, because it is visually challenging to distinguish between "pole" and "small pole," these two classes are merged into a single "pole" category across all three modalities in the dataset.

### B. Implementation Details

**Training parameters.** We train our UniLoc using the Adam optimizer for both instance-level and scene-level matching stages, initializing the learning rate (LR) at  $5e-4$ . The instance pre-training phase consists of training the model for 20 epochs with a batch size of 256. Subsequently, the final model undergoes an additional 20 epochs of training with a batch size of 64. A multi-step training schedule is employed for both instance-level and scene-level training, where the LR is reduced by a factor of 0.4 every 7 epochs. The temperature coefficient  $\tau$  is fixed at 0.1. To encode individual instances within the scene, we leverage PointNet++ [26] as implemented in [16].

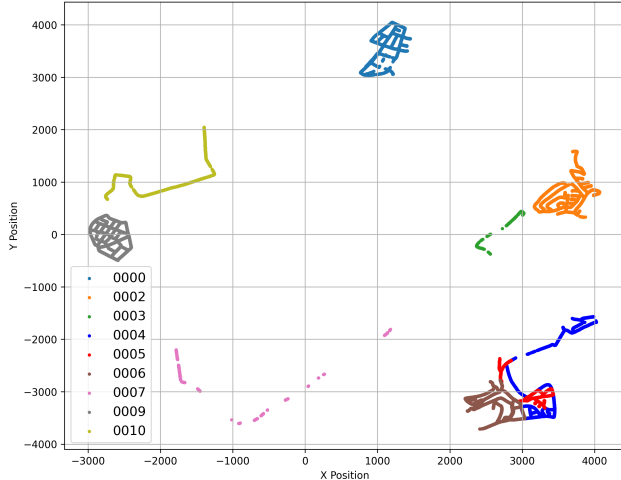


Figure 8. The trajectory distribution of the processed KITTI-360 dataset.

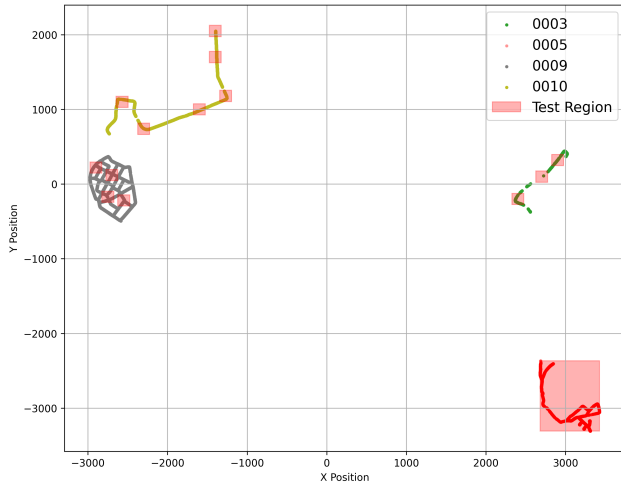


Figure 9. The trajectory distribution of the validation and test sets in the processed KITTI-360 dataset. The red rectangles represent the defined test regions.

**SAP details.** For the Multi-Head Self-Attention (MHSA) used in SAP (as described in Section. 4.2 in main paper), the text branch utilizes a 4-head, 1-layer MHSA, while the point cloud and image branches employ a 4-head, 2-layer MHSA. Furthermore, the Pooling block of Self-Attention-based Pooling (SAP) module for each branch is implemented using a three-layer MLP with a parameter size of 0.13 M.

**Experimental details.** To train and test the model with textual descriptions, we incorporate a tolerance mechanism for scene descriptions. Instead of relying on the descriptions of all instances within a scene, six sentences are randomly selected as the scene’s text description during both training

and testing. This design reflects real-world human behavior, where it is rare to comprehensively describe every instance in a scene without omissions. During training, six sentences are randomly sampled from the descriptions of all instances in a scene to ensure the full utilization of the textual dataset. For testing, the same random seed is used to maintain consistency in results.

For the Image-to-Text task, to ensure a fair comparison, ground-truth semantic masks are excluded during the evaluation phase. Instead, we train a PSPNet [44] model, equipped with a ResNet101 [14] backbone, using paired semantic masks and raw images. PSPNet model (or an equivalent advanced segmentation model) is employed to segment the validation and test sets. During the evaluation of UniLoc, the semantic masks produced by PSPNet are used to segment the raw images, serving as input to the image branch.

### C. Qualitative Analysis

In addition to the quantitative results, we present qualitative examples in Fig. 10, showcasing the place recognition performance among images, point clouds, and corresponding text sampled from the same location. Given any one of these three modalities, UniLoc allows for the retrieval of data from either the same or a different modality. In Fig. 10, we visualize the results for six tasks: LiDAR-to-Image(P2I), LiDAR-to-LiDAR(P2P), Image-to-LiDAR(I2P), Image-to-Image(I2I), Text-to-Image(T2I), and Text-to-LiDAR(T2P). For each task, we display the ground truth of the target modality (the ground truth of target modality sampled from the same location as the query) alongside the top-3 retrieved results. It is worth noting that for I2I and P2P tasks, the query itself is removed from the database, ensuring that the query cannot retrieve itself.

In most cases, UniLoc successfully retrieves target modality data sampled near the query, demonstrating its strong performance in cross-modal place recognition tasks. UniLoc also fails to locate target modality data close to the query in the Top-1 and Top-2 results, as shown in Fig. 10 (T2I). We find that even when the positions of the retrieval results are far from the ground truth, they often contain instances that are visually or semantically similar to them. This highlights the challenge posed by the low diversity of outdoor scenes and suggests that richer and more accurate textual descriptions could help mitigate ambiguity in target modality representations, thereby enhancing localization accuracy.

### D. More Ablation Studies

In this section, we show more experimental results and ablation studies.

**Selection of  $\alpha$ .** In Tab. 5, we examine the impact of different  $\alpha$  values in Eq. 9 (in main paper) on model



Figure 10. Qualitative localization results on the KITTI-360 dataset: In the context of place recognition, the numbers on the top-3 retrieved results indicate the center distances between the retrieved results and the ground truth. The results that were retrieved within 2 meters of the query are highlighted in green, signifying successful localization. Retrievals exceeding this distance are marked in red. Here, P2I denotes LiDAR-to-Image, P2P: LiDAR-to-LiDAR, I2P: Image-to-LiDAR, I2I: Image-to-Image, T2I: Text-to-Image, and T2P: Text-to-LiDAR tasks.

performance. The results indicate that the model achieves optimal performance on both the test and validation datasets when  $\alpha$  is set to 0.3.

Table 5. Hyperparameter analysis in the scene-level matching loss.

$\alpha$	val				test			
	R@1	R@3	R@5	Ave	R@1	R@3	R@5	Ave
0.1	62.7	86.1	92.6	80.5	71.0	91.4	95.3	85.9
0.3	<b>65.6</b>	<b>89.1</b>	<b>94.3</b>	<b>83.0</b>	<b>75.5</b>	<b>95.1</b>	<b>97.9</b>	<b>89.5</b>
0.5	65.4	88.8	93.9	82.7	<b>75.5</b>	<b>95.1</b>	<b>98.0</b>	<b>89.5</b>
0.7	63.3	88.0	93.9	81.7	73.5	94.4	97.6	88.5
0.9	63.1	86.8	92.8	80.9	74.3	94.5	97.7	88.8

### Robustness analysis for the number of textual descriptions.

As shown in Tab. 6 and 7, we explored the impact of textual description richness on model performance. In this experiment, we evaluated the performance of the Text-to-Image and Text-to-LiDAR place recognition using language descriptions containing 4, 5, and 6 sentences, where each sentence corresponds to the description of a single instance. Notably, the size of the textual descriptions used during training remained fixed at six sentences. The Text-to-Image place recognition was tested using ground-truth segmentation masks. We observed that even with text descriptions limited to only 6 sentences, our method achieves a recall performance of 72.5% at top-1 in the KITTI-360

test set, demonstrating its effectiveness. We also believe that adding more descriptive information will further improve performance. Moreover, the findings show that reducing the textual input to five sentences does not significantly impact performance, demonstrating that our UniLoc is robust to a certain extent of missing textual descriptions.

Table 6. Performance comparison of Text-to-Image place recognition on the KITTI-360 dataset with different numbers of instance-level textual descriptions.

Num.	val				test			
	R@1	R@3	R@5	Ave	R@1	R@3	R@5	Ave
6	65.8	89.1	94.5	83.1	72.5	93.6	97.2	87.8
5	49.6	75.5	85.7	70.3	56.7	82.1	89.3	76.0
4	29.9	54.9	67.3	50.7	29.3	52.0	62.5	47.9

Table 7. Performance comparison of Text-to-LiDAR place recognition on the KITTI-360 dataset with different numbers of instance-level textual descriptions.

Num.	val				test			
	R@1	R@3	R@5	Ave	R@1	R@3	R@5	Ave
6	36.4	62.2	73.5	57.4	46.7	73.6	83.3	67.9
5	24.8	46.8	58.6	43.4	30.9	55.1	65.7	50.6
4	12.2	27.9	36.9	25.7	12.5	26.5	35.5	24.8

Table 8. Performance comparison of Image-LiDAR place recognition on the KITTI-360 dataset under different distance thresholds

$d$ (m)	LiDAR-to-Image						Image-to-LiDAR					
	val			test			val			test		
	R@1	R@3	R@5	R@1	R@3	R@5	R@1	R@3	R@5	R@1	R@3	R@5
20	95.4	98.9	99.4	99.0	99.8	99.9	95.0	98.7	99.4	98.9	99.7	99.9
10	93.3	98.5	99.2	98.8	99.7	99.9	92.6	97.9	98.8	98.5	99.6	99.8
5	88.7	96.7	98.6	97.9	99.6	99.8	87.9	96.6	97.9	97.7	99.6	99.8
2	80.0	94.0	97.2	93.1	99.1	99.6	78.4	93.1	96.2	93.6	99.3	99.7

Table 9. Performance comparison of Text-Image place recognition on the KITTI-360 dataset under different distance thresholds

$d$ (m)	Text-to-Image						Image-to-Text					
	val			test			val			test		
	R@1	R@3	R@5	R@1	R@3	R@5	R@1	R@3	R@5	R@1	R@3	R@5
20	93.7	98.4	99.6	94.5	98.5	99.3	93.0	98.4	99.2	94.5	98.5	99.1
10	90.7	97.9	99.2	93.9	98.2	99.1	90.1	97.8	98.9	93.7	98.1	99.0
5	86.5	96.5	98.7	91.9	97.8	98.9	85.2	97.1	98.3	91.4	97.6	98.7
2	78.3	94.0	97.2	85.9	96.7	98.4	76.1	93.5	96.5	84.6	96.2	98.2

**Place recognition under different distance thresholds.**

In this ablation study, we regard the retrieved result as a correct match if the distance is within  $d$ . To evaluate UniLoc’s cross-modal place recognition capabilities between images and LiDAR (Image-to-LiDAR, LiDAR-to-Image tasks), we set the  $d$  at four different values ranging from 20 m to 2 m. Note that we do not exclude cross-modal data from the same sampling location as the query in the database. As shown in Tab. 8, Image-to-LiDAR place recognition achieves the best performance not only at the  $d = 20m$  but also maintains a good recall rate even under the strict 2 m threshold.

For Image-to-Text and Text-to-Image place recognition, we conducted experiments under the same conditions, as shown in Tab 9. These results indicate that our UniLoc has strong cross-modal generalization capabilities across different input types under different distance thresholds.

**Comparison with different backbones used in scene-level matching.**

To evaluate whether the pre-trained CLIP[28] is the most suitable backbone, we also experimented with replacing the CLIP with the BLIP[18] to encode text and images. Notably, we do not utilize any pre-trained instance-level models here. Follow the same methodology as described in Section 6.3 of the main paper, where performance is averaged across Text-Image (Text-to-Image and Image-to-Text tasks) and Image-LiDAR (Image-to-LiDAR and LiDAR-to-Image tasks) place recognition. All experiments were conducted using 2D ground-truth semantic labels. The results are presented in Tab. 10. We can see

that upgrading the backbone from CLIP to a more advanced model like BLIP can significantly enhance UniLoc’s overall performance. Therefore, we believe that integrating even more powerful models, such as BLIP2 [19], could further boost its capabilities. This finding also highlights our UniLoc can fully leverage recent advances in large-scale contrastive learning.

Table 10. Performance comparison with different backbones used in scene-level matching.

Backbone	val				test			
	R@1	R@3	R@5	Ave	R@1	R@3	R@5	Ave
CLIP [28]	62.7	86.6	92.8	80.7	71.3	92.4	96.2	86.6
BLIP [18]	<b>63.1</b>	<b>87.3</b>	<b>93.4</b>	<b>81.3</b>	<b>73.1</b>	<b>93.6</b>	<b>96.9</b>	<b>87.9</b>